

Reactive processing of titanium carbide with titanium

Part 1 *Liquid-phase sintering*

CANDACE JO QUINN,* DAVID L. KOHLSTEDT

Department of Materials Science and Engineering, Cornell University, Ithaca, NY 14853, USA

The reactive sintering of titanium carbide with titanium metal was studied using mechanical mixtures of fine-grained powders heated in vacuum above the TiC–Ti eutectic temperature. Mixtures with bulk compositions of TiC_{0.94} to TiC_{0.63} yielded nonstoichiometric carbide with less than 0.5 wt % residual titanium metal after sintering, while residual metal was observed at higher titanium concentrations. The effects of time, temperature, and composition on Mohs hardness, final porosity and final grain-size were determined using a Box–Wilson experimental design. The experimental ranges studied were sintering times of 10 to 100 min, sintering temperatures of 1650 to 1850° C, and compositions from TiC_{0.94} to TiC_{0.58}. Over these experimental ranges, the effects of time and temperature were small compared with those of composition. The Mohs hardness increased approximately linearly from two to nine with increasing percentage of titanium metal in the starting powder. The average grain size ranged from 15 to 70 μm, increasing with increasing time and temperature. For bulk compositions TiC_{0.94} to TiC_{0.70} grain growth was largely due to the conversion of titanium to substoichiometric carbide which grows epitaxially on the carbide grains. Substantial grain growth occurred for higher metal concentrations. The open porosity decreased from 28% to 16% as the amount of titanium metal in the starting powders was increased. Both the grain growth and the densification during reactive sintering of titanium–titanium-carbide mixtures were analysed in terms of a sintering model adapted from Kuczynski. A factor which empirically describes the behaviour of the system over a range of compositions was incorporated into the equations proposed by Kuczynski. Microstructural evidence and the activation energies for grain growth and densification all indicate that the rapid reaction between titanium metal and titanium carbide to form substoichiometric carbide occurs via short-circuit diffusion of carbon out of the carbide grains along Ti₂C platelets. Low sintered densities are attributed to the rapid formation of a solid titanium-carbide skeleton which prevents significant particle rearrangement in the eutectic liquid. Solution–precipitation processes do not appear to contribute significantly to the densification in this system.

1. Introduction

Transition-metal carbides form a class of extremely hard, refractory materials. The microhardness of the carbides, 20 000 to 30 000 MPa, is intermediate between alumina, 18 000 MPa, and diamond,

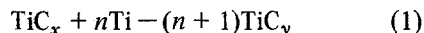
70 000 MPa. The melting points of the transition-metal carbides are in the range 2000 to 4000° C [1]. These two properties make the transition-metal carbides attractive for wear-resistant parts such as cutting tools and extrusion dies and for

*With Corning Glass Works, Ceramic Research Department, Sullivan Park, Corning, NY 14831, USA

high-temperature applications such as nozzles and turbines in jet engines. However, these same properties impose significant manufacturing difficulties. High-purity powders of carbides sinter very poorly, even at temperatures approaching the melting point.

The approach most widely used to facilitate densification of various carbides is to sinter carbide particles with 5 to 40 wt% of a metal such as nickel, cobalt or iron which melts at approximately half the melting point of the carbide. The base-metal binder phase greatly enhances the fracture toughness of the cermets, a property which is important for uses such as cutting tools; however, high-temperature application of cermets is limited by the melting point of the binder phase [2].

Titanium carbide, like the other group IV and V transition-metal monocarbides, exists with the NaCl structure over a very wide range of carbon-metal ratio, $\text{TiC}_{0.97}$ to $\text{TiC}_{0.47}$ [3]. This wide range of composition suggests that it might be possible to produce high-density, single-phase titanium carbide by the reactive liquid-phase sintering of mixtures of nearly stoichiometric titanium carbide and titanium metal:



where $y = x/(n + 1)$. Such a material might find high-temperature applications while being as easily fabricated as the base-metal cermets.

In the present paper, the effects of sintering times and temperature on final porosity and grain size are determined over a range of compositions. Models describing the sintering behaviour are developed as extensions of a statistical sintering model presented by Kuczynski [4]. The resulting equations describe sintering in a multiphase, reactive system. The reaction and sintering mechanisms are deduced from microstructural observations, determination of phases present, and observed activation energies for grain growth and densification.

2. Experimental design

Two experiments are reported in the present study. The first experiment (experiment A) examined liquid-phase reactive sintering of titanium-titanium carbide compacts as a function of composition only. Samples of bulk compositions TiC_x - where $x = 0.94, 0.84, 0.75, 0.69, 0.63$ and 0.58 - were fired simultaneously at 1750°C

for 1 h. The second experiment used a design (Fig. 1) developed by Box and Wilson [5] to study the liquid-phase reactive sintering of titanium-titanium carbide mixtures. The independent variables were sintering time, t , sintering temperature, T , and the bulk carbon-titanium ratio, C . The dependent or response variables measured on the sintered samples were porosity, average grain size, Mohs hardness, and phases present. The temperatures chosen, 1650 to 1850°C , were all above the eutectic temperature. The sintering times covered one order of magnitude, 10 to 100 min. The bulk compositions, $\text{TiC}_{0.94}$ to $\text{TiC}_{0.58}$, were in the single phase TiC region of the phase diagram. The sintering schedules were run in random order to avoid biasing the results.

The Box-Wilson is a composite experimental design. It is built up of a two-level factorial, i.e. the points which lie on the corners of the cube in Fig. 1, plus star points. The star points in this experiment were chosen such that the distance from the centre point is equal to the distance of the factorial points from the centre. Thus, all of the experimental points lie on a sphere in time-temperature-composition space. If the steps chosen for each independent variable are approximately equal in the magnitude of their effect on the response variable(s), then an unbiased view of the response surface is obtained because the variance is equal in magnitude in all directions.

This experimental design compares favourably with three-level factorials in terms of the precision with which a regression equation can be fitted to the data and in terms of its ability to evaluate the interactions between the independent variables and higher-order terms. A first-level interaction between time and composition, for example, might mean that the grain growth of high-titanium samples as a function of time differed from that of low-titanium samples.

The inclusion of a higher-order term means that the response surface is curved and that a response variable is better described by a term such as t^n or T^m . The advantage of the Box-Wilson design is that it requires only fifteen runs, while a three-level full factorial requires twenty-seven runs for the three independent variables being studied.

Four replicates were run at the centre point of the Box-Wilson experiment. These replicates provide an estimate of the random errors which might arise from measurement errors in either the independent or the response variables. Replicating

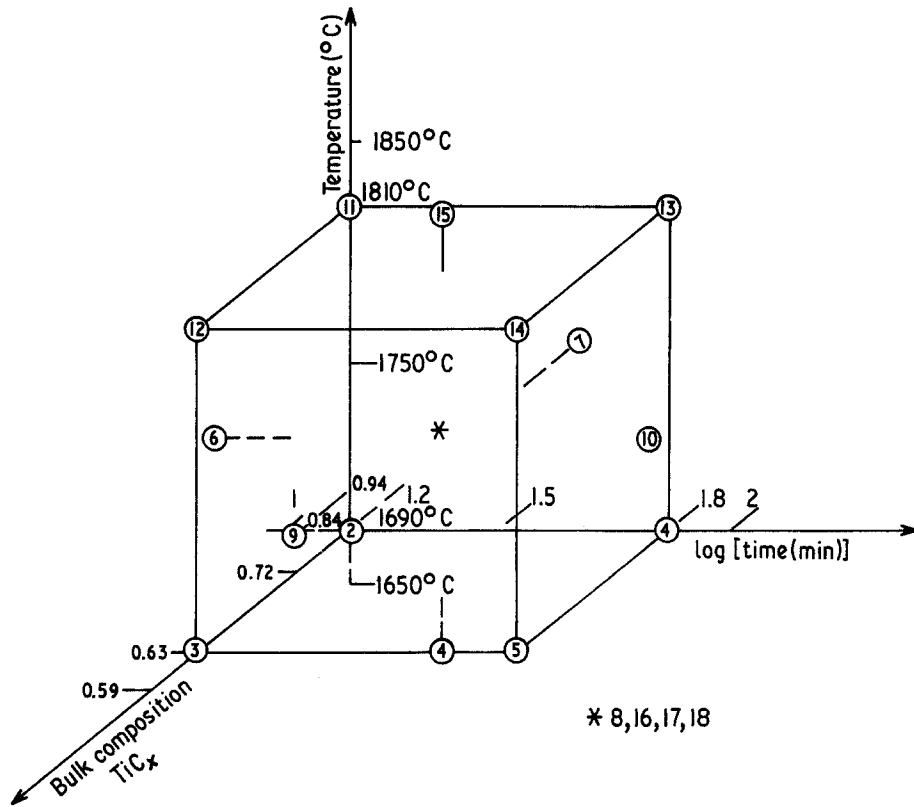


Figure 1 Box-Wilson experimental design. The positions of the circles indicate the experimental conditions used in sintering experiment B. The numbers within the circles are the sample identification numbers used in Table III.

the centre point gives a good estimate of the errors over the range of the independent variables with a minimum number of runs. After the data were examined, four additional samples were prepared from compositions between $\text{TiC}_{0.66}$ and $\text{TiC}_{0.56}$ and sintered at 1750°C for 63 min to better quantify a sharp change in slope in the grain size against composition data in this composition region.

The data generated from the sintering experiment were interpreted in terms of a sintering model adapted from the literature [4]. The modelling was done by least-squares linear regression. The goodness of fit was judged in two ways. First the residuals or the differences between observations and predictions, $Y - \hat{Y}$, were examined. A good model is characterized by small residuals of random sign. Residuals which are not randomly positive and negative indicate that there is curvature in the data for which the model does not account. The size of the residuals is evaluated by calculating the residual mean square, S_r^2 :

$$S_r^2 = [\Sigma \hat{Y}^2 + \Sigma (Y - \hat{Y})^2] / (n - 1) \quad (2)$$

where n is the number of observations and $(n - 1)$ is the degrees of freedom. The residual mean square from regression is then compared with the variance of the replicates by a standard statistical variance ratio or F test to determine whether these two estimates of variance are significantly different

$$F = S_1^2 / S_2^2 \quad (3)$$

where S_1 is always the larger of the two variances. The calculated value of F is compared with the values of F which could be obtained due to sampling variations at given levels of probability and for various degrees of freedom [6]. These expected values of F are tabulated in numerous statistical texts and mathematical handbooks. Second, the square of the multiple correlation coefficient, R^2 , is examined. If more variables are included in the regression equation then R^2 will increase, even if the variable added is of no real value. To compensate for this effect, the value of R^2 corrected for degrees of freedom is calculated as

$$R^2 = 1 - \frac{[\Sigma \hat{Y}^2 + \Sigma (Y - \hat{Y})^2] / (n - p)}{(Y - \hat{Y}) / (n - 1)} \quad (4)$$

where p is the number of coefficients fit in the regression equation [7].

3. Experimental methods

The titanium and titanium-carbide powders used in this experiment had average particle sizes, as measured by Coulter counter, of 10 and 7 μm , respectively. The particle-size distributions are shown in Fig. 2. The carbon and oxygen levels were measured by decomposing the samples under oxidizing or reducing conditions, respectively, and analysing the evolved gases by infrared spectroscopy. The sample purity was determined by flame-emission spectroscopy. As indicated in Table I, oxygen was a primary contaminant in both powders. Some metal impurities (Fe, Co and Ni) were detected, presumably arising from milling operations during the manufacture of the powders. The carbon-metal ratio of the TiC powder was 0.94.

Titanium-carbide and titanium powders were mixed by tumbling in nalgene jars for a minimum of 16 h. 10-g pellets were cold pressed in a 2 cm die at 14 MPa (2000 psi). These pellets were sintered in a tungsten-element furnace under a vacuum of less than 2×10^{-4} torr. A W/W-26%Re thermocouple was used to record temperatures less than 1800°C. Optical pyrometry was used at higher temperatures. Temperatures were controlled to $\pm 5^\circ\text{C}$. Heating and cooling rates were $50^\circ\text{C min}^{-1}$ throughout the study.

Polished sections of sintered samples were etched and stained for 15 to 30 sec in a 1:1:4 solution of nitric, hydrofluoric and lactic acids. Optical micrographs were taken in reflected light. Grain sizes were determined on the photomicro-

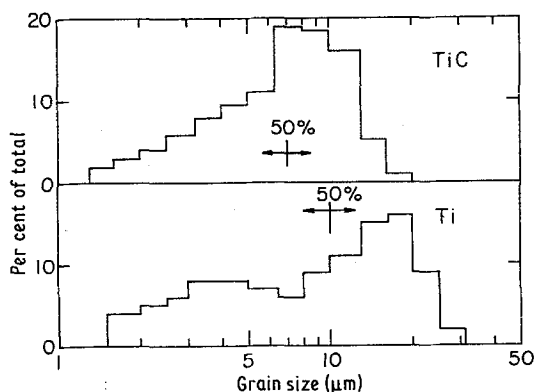


Figure 2 Particle-size distribution of starting powders determined by Coulter counter.

TABLE I Chemical analysis of starting powders

Sample	Element	Concentration (wt %)
TiC	C	18.5
	O	0.91
	Co	0.01 to 0.1
Ti	Ni	0.01 to 0.03
	C	0.12
	O	2.29
	Fe	1.0 to 3.0
	Ni	0.03 to 0.1
	Cr, Mg	0.01 to 0.03

graphs using a line-intercept technique with a correction factor of 1.5 [8]. Mean grain sizes and standard deviations were calculated from fifty line-intercept measurements for each sample.

Hardness was measured using the Mohs scale [9]. This comparative scratch test, which uses minerals of known hardness, was chosen in preference to microhardness measurements because it provides an indication of the strength of bonding between particles rather than the hardness of individual grains. The Mohs scale is a linear hardness scale for values of nine and below. Single crystals of titanium carbide have a hardness of nine on the Mohs scale.

Open porosity, skeletal density and bulk density were measured by Archimedes' principle on samples which had been dried to constant weight.

X-ray diffraction was used to determine the crystalline phases present and to estimate the relative proportions of those phases. Diffractometer traces were obtained on powder samples for values of 2θ from 10 to 60 at 2°min^{-1} . The peak height of the strongest line of titanium, (011) at $2\theta = 40.3^\circ$, was used to estimate the amount of residual titanium metal. Diffraction peak heights measured on sintered samples were compared with a calibration curve, shown in Fig. 3, which was generated using unsintered mixtures of titanium carbide and titanium metal. The limit of detection by this method was 0.5 wt % residual titanium. Lattice parameters were calculated from the (224) line of TiC at $2\theta = 121^\circ$ using an internal silicon standard.

4. Experimental results

4.1. Experiment A: the effect of composition

The crystalline phases, grain size, Mohs hardness and porosity of the sintered samples from exper-

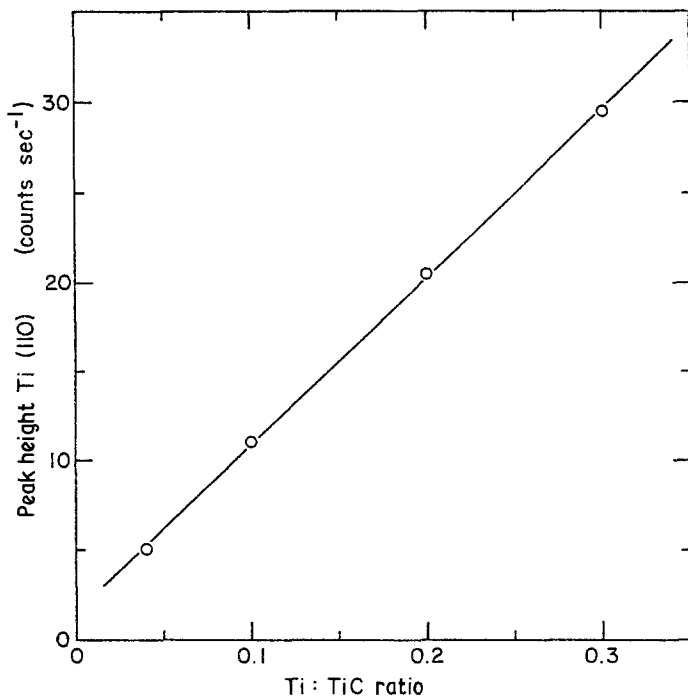


Figure 3 X-ray diffraction calibration curve for determining the amount of residual titanium metal in sintered samples.

iment A, which studied the effects of composition, are tabulated in Table II. The bulk compositions of these samples lie in the single-phase TiC field. X-ray diffraction data demonstrate that TiC is the major crystalline phase in all of the sintered samples. The lattice parameter for each sintered samples is plotted in Fig. 4 as a function of bulk composition. A small extra diffraction peak at ~ 0.213 nm was observed in the sintered sample with a bulk composition of $\text{TiC}_{0.63}$. The $\text{TiC}_{0.58}$ sample (35 wt% titanium metal in the starting mixture) contained 17 wt% residual metal. The metal was observed at triple junctions and along grain boundaries.

Optical micrographs showing the sintered microstructures of sintered samples $\text{TiC}_{0.69}$,

$\text{TiC}_{0.63}$ and $\text{TiC}_{0.58}$ are presented in Fig. 5. Note the intragranular texture evident in the micrographs. Coalescence of pores was pronounced in the high titanium samples. Large (> 1 mm) well-rounded pores are numerous in the $\text{TiC}_{0.58}$ sample. The pore size in the $\text{TiC}_{0.58}$ sample is approximately four times that in the $\text{TiC}_{0.63}$ sample.

The open porosity is plotted as a function of bulk composition in Fig. 6. These data indicate that the open porosity of the sintered samples decreases smoothly with increasing titanium content.

The grain size increased very little during the sintering of samples with C-Ti ratios greater than 0.65. However, as is clearly seen in Fig. 7, grain growth was pronounced at higher titanium levels.

TABLE II Experiment A: Ti-TiC compacts sintered at 1750°C for 1 hour

Sample	Bulk C-Ti	Grain size (μm)	% open porosity	Mohs hardness	Residual Ti (wt %)
A1	0.94	13	32	2	n.d.
A2	0.84	13	30	4.5	n.d.
A3	0.75	14	29	5	n.d.
A4	0.69	13	26	8.5	n.d.
A5	0.63	35	21	9	$> 1^{*\dagger}$
A6	0.58	75	17	8.5	$17^{*\dagger}$

* Intragranular texture.

\dagger XRD peak at 0.213 nm.

n.d. = none detected.

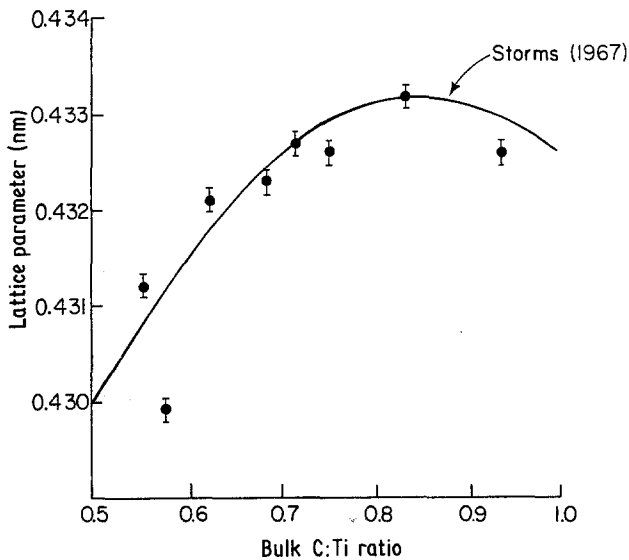


Figure 4 Lattice parameter of sintered TiC as a function of composition.

The Mohs hardness as a function of composition is plotted in Fig. 8. The Mohs hardness, H , increases approximately linearly with increasing metal content in those samples which have less than 1 wt % residual metal. The equation obtained by a least squares fit to the data is

$$H = 21.1 - 20.1C \quad (4)$$

with $R^2 = 87.7\%$, corrected for degrees of freedom, where the composition, C , is expressed as the bulk carbon-titanium ratio.

The initial or green density of the powder compacts was found to be a linear function of carbon-titanium ratio, as indicated in Fig. 9.

4.2. Experiment B: effects of time, temperature and composition

A second series of samples (experiment B) were prepared to examine the roles of sintering time and temperature, as well as C-Ti ratio, on the final porosity and grain size. The results of this

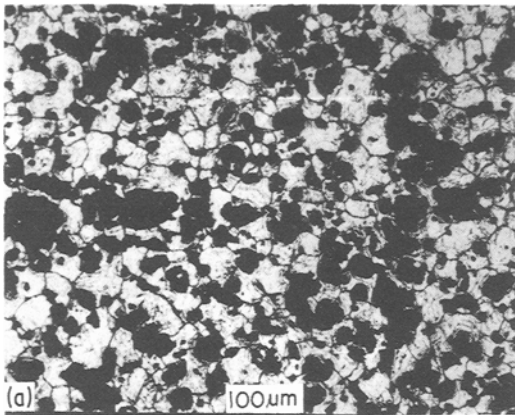
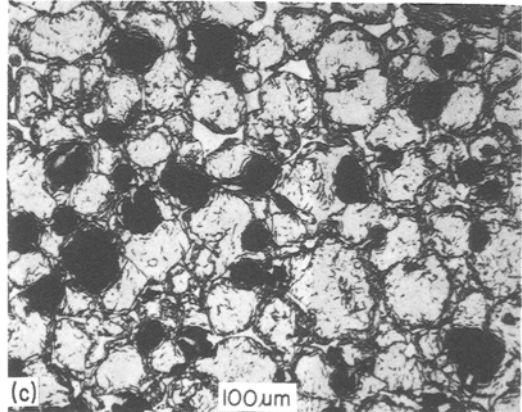
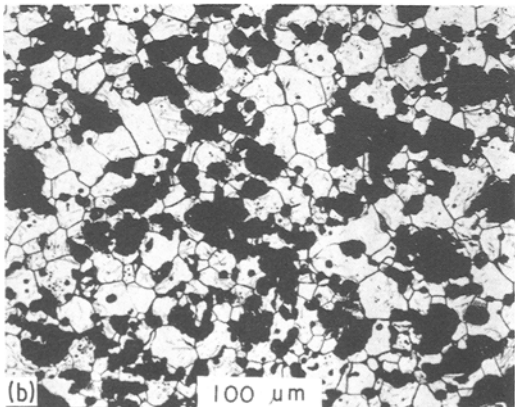


Figure 5 Optical micrographs of etched surfaces of samples from experiment A. The samples were all sintered in vacuum at 1750°C for 1 h. The compositions of the samples were (a) TiC_{0.69}, (b) TiC_{0.63}, (c) TiC_{0.58}.



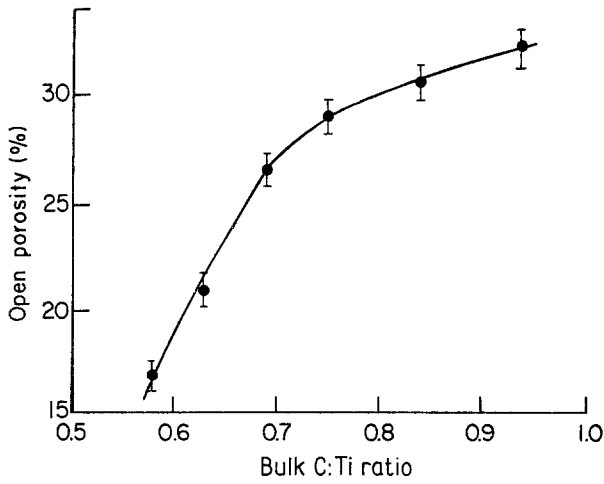


Figure 6 Open porosity against composition for the sintered Ti-TiC samples of experiment A.

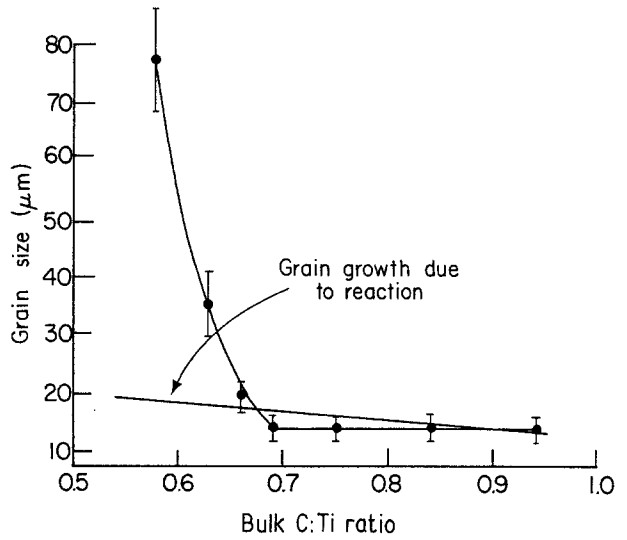


Figure 7 Mean grain size against composition for the sintered TiC samples of experiment A. The grain growth which occurs simply by the conversion of titanium metal to titanium carbide is indicated.

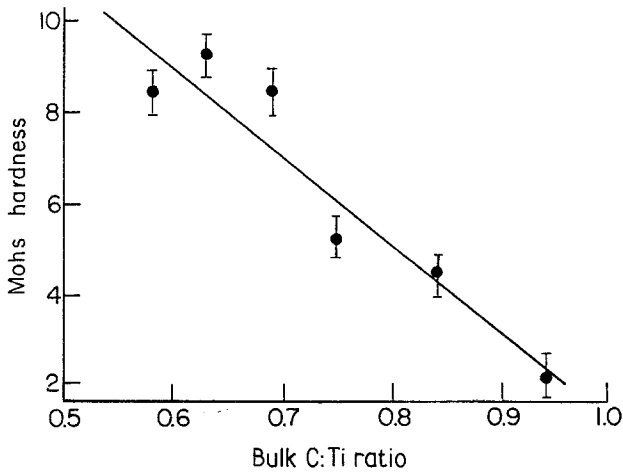


Figure 8 Mohs hardness against composition for sintered samples from experiment A.

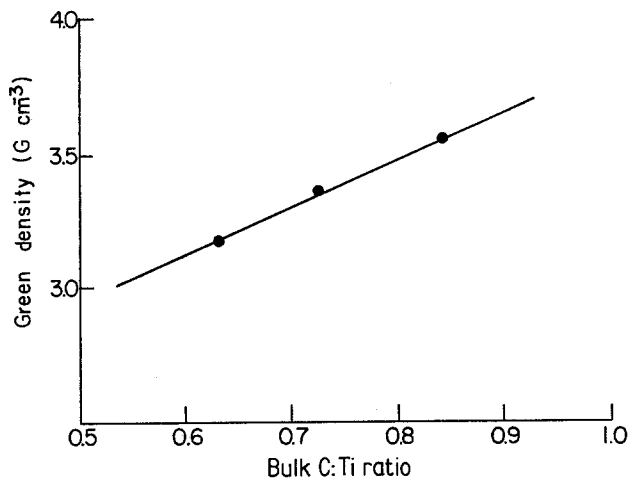


Figure 9 Green density against composition for cold pressed 10 g pellets used in sintering studies.

experiment are tabulated in Table III. The open porosity ranged from 28% to 17% for all but the high titanium sample, B9. The coalescence of pores in sample B9 was extreme, leading a non-uniform distribution of pores larger than 1 mm in diameter. Due to this nonuniform distribution of pores, the open porosity of 6% and total porosity of 13% measured for a piece of this sample may not be representative of the average porosity.

The measured grain sizes ranged from 15 to 68 μm . Grain size is a strong function of composition. This result is shown in Fig. 10 where data for all times and temperatures are plotted. The data points collected in addition to those specified by the Box-Wilson design (i.e. samples 19B to 22B) were chosen to better quantify the change in slope of the grain size against C-Ti ratio plot.

In all cases the X-ray diffraction data indicate

TABLE III Experiment B: the effects of time, temperature and composition

Sample	Temperature (°C)	Time (min)	Bulk C-Ti	Grain size (μm)	% open porosity	Relative density
A1	1650	32	0.72	19.6	25.7	0.72
A2	1690	16	0.84	15.4	27.7	0.70
A3	1690	16	0.63	19.6	23.4	0.76*†
A4	1690	63	0.84	17.0	25.4	0.71
A5	1690	63	0.63	31.7	20.3	0.79*†
A6	1750	10	0.72	15.5	27.8	0.71†
A7	1750	32	0.94	17.0	24.0	0.73
A8	1750	32	0.72	22.1	23.0	0.77
A9	1750	32	0.58	57.6	6.3‡	0.87
A10	1750	100	0.72	23.8	21.7	0.77
A11	1810	16	0.84	16.8	24.7	0.72
A12	1810	16	0.63	37.3	21.4	0.78*
A13	1810	63	0.84	20.4	23.9	0.72
A14	1810	63	0.63	37.6	18.0	0.81*‡
A15	1850	32	0.72	22.2	20.5	0.77
A16	1750	32	0.72	16.9	24.7	0.73
A17	1750	32	0.72	19.3	23.4	0.74
A18	1750	32	0.72	20.4	23.2	0.74*
A19	1750	60	0.66	27.5	20.6	0.76‡
A20	1750	60	0.61	45.8	17.9	0.80‡
A21	1750	60	0.59	51.8	20.0	0.79‡
A22	1750	60	0.56	67.7	16.6	0.84‡

*XRD line at 0.213 nm.

†Intragranular texture.

‡Sample contains large, > 1 mm, pores.

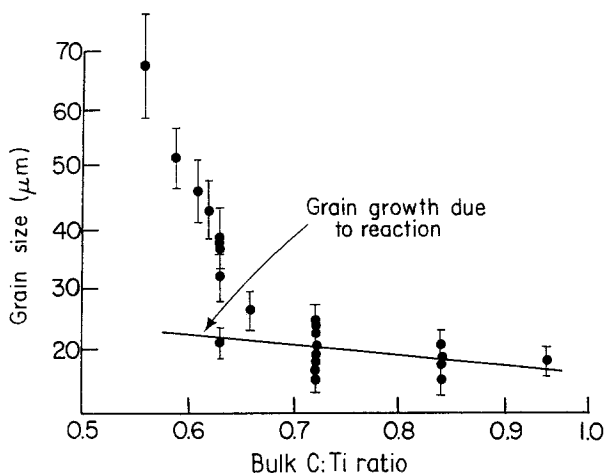


Figure 10 Mean grain size against composition for sintered samples from experiment B. Data for all of the sintering times and temperatures have been plotted. The grain growth which is expected to result from the conversion of titanium metal to carbide is indicated.

that TiC is the major crystalline phase present. Residual metal, 3 wt %, was detected only in the highest titanium sample, B9. In some samples a small X-ray diffraction peak (less than 2% relative intensity) at approximately 0.213 nm appeared on the shoulder of the TiC (200) peak, 0.217 nm. Those samples in which a diffraction peak at 0.213 nm was detected are indicated in Table III.

Optical micrographs of samples B3 and B9 are shown in Figs. 11a and b. In sample B9, residual titanium metal is observed at the triple junctions. The texture in the interior of the grains in both micrographs suggests the possible presence of a minor amount of a second phase. Those samples with this intragranular texture are indicated in Table III.

5. Modelling of the sintering process

A variety of processing parameters including time,

temperature, composition, particle size, particle shape, green density and firing atmosphere are important in the sintering process. The problems of understanding the mechanisms and kinetics of sintering are largely due to the complexity of systems of practical interest. Particles are always to some extent irregular in shape, nonuniform in size, impure, inhomogeneously packed and so on.

The approach most frequently employed in the modelling of sintering is to make simplifying assumptions about the particle geometry and then to develop models for specific sintering mechanisms or specific stages of the sintering process [10]. The result of these simplifications is that experimental verification of any sintering model is difficult and open to debate; and application of sintering models to more complicated systems, such a multiphase reactive mixtures, has generally not been attempted.

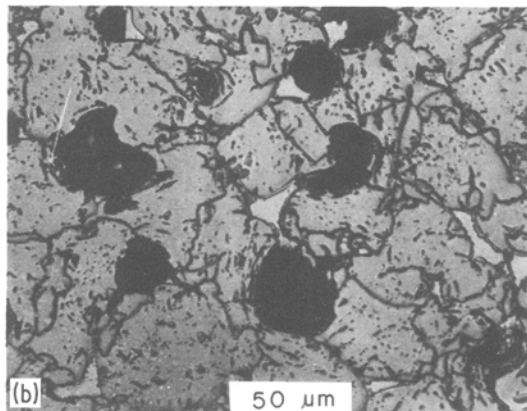
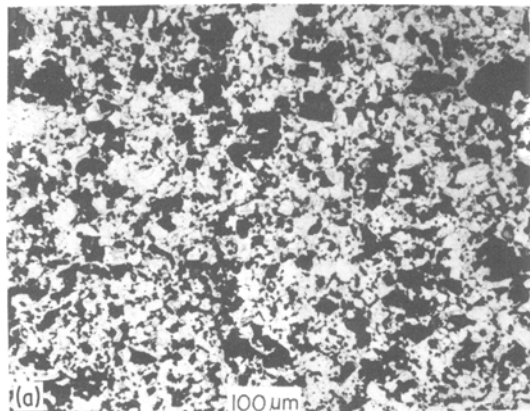


Figure 11 Optical micrographs of polished and etched section of sintered TiC samples: (a) sample B3, (b) sample B9.

A less widely used approach introduced by Kuczynski [4] applies the methods of statistics to a more general model which is developed for a distribution of particle sizes. It is this model which we will examine in connection with the present study. The first equation of interest for the present study describes the grain size, a , as a function of time, t , initial porosity, P_0 , and starting grain size, a_0 :

$$a^{n_2} - a_0^{n_2} = \left[\frac{K^3 V_0 g^2}{P_0^{1-x}} \right]^{s-1/2x} \frac{n K_0 \phi \alpha t}{P_0^s} \quad (5)$$

where V_0 is the average pore volume at $t = 0$; ϕ is the probability of a pore having the proper neighbourhood for shrinkage; K_0 comes from Zener's relationship, $a = K_0 r / P$, where r is the average pore size; $\alpha = 8\pi\gamma\Omega D / [kT]$ where γ is the boundary energy, Ω is the atomic volume, and D is the diffusion coefficient for the process(es) which contribute to sintering; g is a geometric factor relating the average pore volume, V_0 , to the average pore radius.

Kuczynski notes that Equation 5 is often observed to reduce to

$$a^3 - a_0^3 = (1+x)K\phi\alpha t / P_0. \quad (5a)$$

The second equation of interest for Kuczynski's work describes the porosity:

$$\frac{1}{P^{n_1}} - \frac{1}{P_0^{n_1}} = \frac{n\phi\alpha P_0^{2-n_1} t}{g^2 K_0^2 V_0}. \quad (6)$$

Equations 5 and 6 can be combined to give the third equation required to analyse the present sintering data:

$$a P^{n_3} = a_0 P_0^{n_3}. \quad (7)$$

The exponents in Equations 5, 6 and 7 are related by

$$n_1 = n_2 n_3. \quad (8)$$

These three equations from Kuczynski [4] are similar to, but more general than, many of the sintering models in the literature. The equations were developed for single-phase, solid-state sintering. Modifications must be made to describe liquid-phase reactive sintering of titanium-titanium carbide compacts over a range of composition. Let us examine those features which might be sensitive to changes in composition. In Equations 5 and 6 changes in the Ti-TiC ratio effect P_0 because increasing the titanium level is observed to increase the green density. V_0 would likewise be influenced by changes in composition. γ is also

expected to be a function of composition. We shall therefore look for functions of composition, $A(C)$, which describe the composition-dependent behaviour of K_0 , P_0 , V_0 , and γ such that Equations 5 and 6 can be rewritten for the present study in the form

$$a^{n_2} - a_0^{n_2} = A(C)Dt/T; \quad (5b)$$

$$1/P^{n_1} - 1/P_0^{n_1} = A_1(C)Dt/T. \quad (6a)$$

Examination of the shape of the grain size versus composition curves in Figs. 7 and 10 suggests that a power function is a reasonable empirical choice for the functions $A(C)$. The equations by which we will attempt to model the present sintering data are therefore Equation 7 and

$$a^{n_2} - a_0^{n_2} = A_2 C^p \exp(-Q/RT)t/T; \quad (5c)$$

$$1/P^{n_1} - 1/P_0^{n_1} = A_3 C^p \exp(-Q/RT)t/T. \quad (6b)$$

6. Application of sintering models to data

To obtain a relationship between grain size and porosity, the following data were fitted to Equation 7. Values for final open porosities are listed in Table III. Values of initial porosity were calculated from the green densities plotted in Fig. 9 and therefore represent a lower limit for P_0 . In these equations, P_0 applies to pores which are already rounded. With liquid titanium present, rounding occurs in the first few minutes of sintering. In the same short time, mechanical rearrangement of particles can take place so that the true value of P_0 may be somewhat lower than the value used in this analysis. The final grain sizes are listed in Table III.

A least-squares linear regression of the final open porosity, green density, and final grain-size data are given by

$$a/14.3 \mu\text{m} = (P_0/P)^{1.74} \quad (7a)$$

with $R^2 = 88.4\%$, adjusted for degrees of freedom. The value of a_0 calculated from the regression analysis, $14.3 \mu\text{m}$, is in good agreement with the particle size of the starting powders. It is also consistent with the final grain size observed for samples sintered with no metal additions which were very porous and therefore experienced little or no grain growth. A plot of grain size versus P/P_0 is provided in Fig. 12.

The grain growth data were fitted to Equation 5c by taking the logarithm of both sides of this equation,

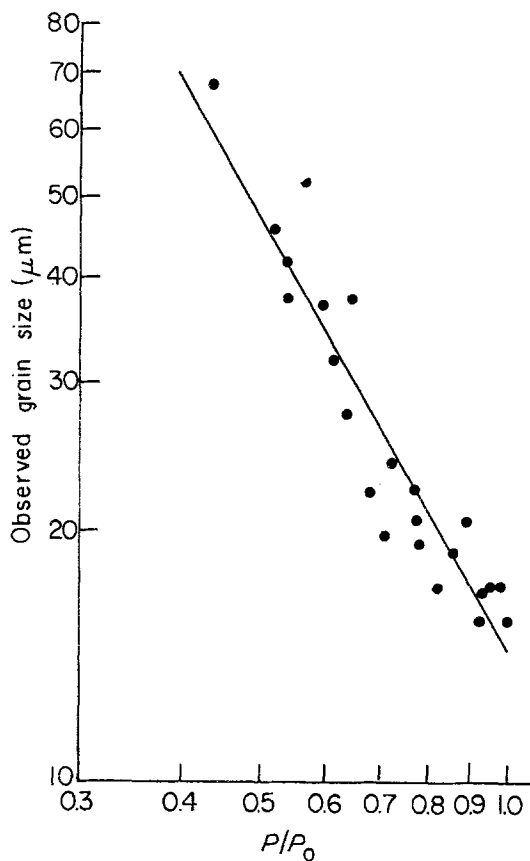


Figure 12 Mean grain size against porosity. The line is a least-squares fit of the data to Equation 7. The intercept gives a value of $14.3 \mu\text{m}$ for the initial grain size and the slope of the line gives the value of 1.74 for the exponent n_3 in Equation 7.

$$\ln(a^{n_2} - a_0^{n_2}) = \ln(A) + q \ln(t) + p \ln(C) + r \ln(1/T) - Q/RT \quad (5d)$$

The model we have adopted predicts that the values of q and r in Equation 5d should be 1; but it is convenient to introduce these exponents for the purpose of performing the least-squares linear regression. Using the value of $a_0 = 14.3 \mu\text{m}$ determined above and the final grain-size data listed in Table III, the best linear-regression fit was obtained for $n_2 = 3$. Including the $\ln(1/T)$ term in Equation 5d did not improve the regression. The value determined for q was 1.06, in excellent agreement with the model. The final regression equation obtained from Equation 5d is

$$a^3 - a_0^3 = 6 \times 10^{-7} \text{cm}^3 \text{sec}^{-1} \times \exp[(-260 \text{kJ M}^{-1})/RT] t C^{-9} \quad (5e)$$

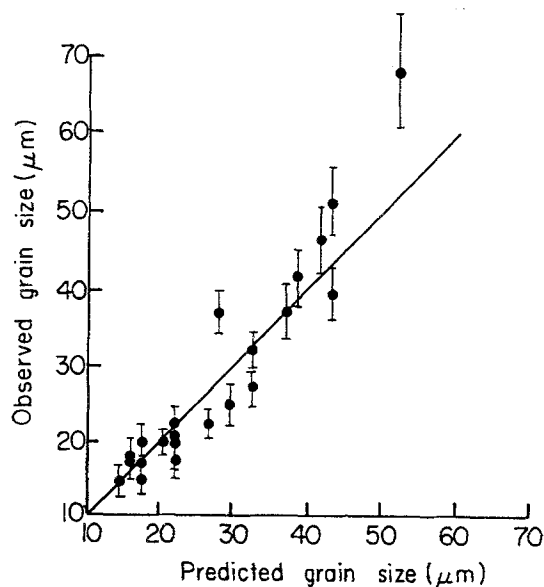


Figure 13 Observed grain size against values calculated from Equation 5e. The solid line represents equality of the observed and predicted values.

with $R^2 = 84.9\%$, corrected for degrees of freedom. The grain-size data are well described by Equation 5, as is illustrated graphically in Fig. 13, where the observed grain size is plotted against that predicted by Equation 5e.

Equations 5e and 7 can be combined to describe the porosity:

$$(P_0/P) - 1 = 6 \times 10^{-7} \text{cm}^3 \text{sec}^{-1} \times \exp[(-260 \text{kJ M}^{-1})/RT] t a_0^{-3} C^{-9} \quad (6c)$$

The observed values of P/P_0 are plotted in Fig. 14 against the values predicted by Equation 6c to give an indication of the quality of the fit of this model to the experimental data.

7. Discussion

The dependence of grain size and porosity on composition in Equations 5e and 6c are useful in that it quantifies the data, but must be considered more carefully in order to understand the processes which are being described. The relationship between final grain size and composition, plotted in Figs. 7 and 10 for experiments A and B, is best understood as two linear functions of composition, although it can be mathematically described as a power-law function of composition. At compositions between $\text{TiC}_{0.94}$ and $\text{TiC}_{0.70}$ grain

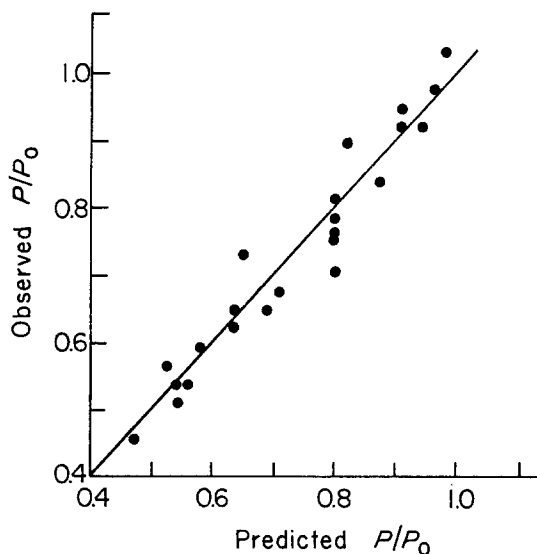


Figure 14 Observed porosity against values calculated from Equation 6c. The line represents a one-to-one correspondence between observations and predictions.

growth is due largely to the reaction of titanium metal with titanium carbide to form an epitaxial shell of substoichiometric carbide around the original titanium carbide grains [11]. The grain growth due to this reaction was calculated as a function of composition using the molar volumes of TiC which can be determined from the composition and the lattice parameters plotted in Fig. 4. The starting grain size was taken to be $14\ \mu\text{m}$ from the value calculated from Equation 7. At bulk compositions higher in titanium than $\text{TiC}_{0.70}$ there is a marked increase in grain growth with increasing metal content.

In Fig. 10 the grain size against composition data for all of the samples (i.e. for all of the sintering times and temperatures) fall on the same curve as those of experiment A plotted in Fig. 7. Sintering time and temperature appear to have no effect on the location of the inflection point in Figs. 7 and 10. Therefore the marked increase in the rate of grain growth at bulk compositions with $x < 0.70$ must be due to a compositional effect.

One possible explanation for the accelerated growth rate at higher metal levels is that the liquid phase exists long enough during the sintering process to promote densification and to allow accelerated grain growth via diffusion through the liquid phase. Two points deserve comment, however. First, for 21 vol% metal in the starting mixture (bulk composition = $\text{TiC}_{0.72}$) all of the metal

has disappeared in less than 10 min at 1750°C (sample B6). For 31 vol% metal in the starting mixture (bulk composition = $\text{TiC}_{0.63}$) all of the metal has disappeared in less than 16 min (sample B3). Thus, most of the samples whose values are plotted in Figs. 7 and 10 had liquid titanium metal present for only a small fraction of the sintering time. Only samples A6 and B9 which started with 35 vol% metal phase contained unreacted metal at the end of the sintering cycle at 1750°C . If grain growth and densification were accelerated by diffusion through the liquid, these samples might be expected to represent discontinuities in the curves of grain size and porosity against composition (Figs. 6, 7 and 10) and to have grain sizes substantially larger and porosities notably smaller than observed. We conclude, therefore, that diffusion through the liquid phase and solution-precipitation processes play little or no role in the sintering of titanium-titanium carbide compacts. Second, changes in sintering temperature did not shift the inflection point in the curves of grain size against composition, even though the rate of disappearance of the titanium metal increases with increasing temperature [11]. If grain growth was enhanced by diffusion through the liquid then at higher temperatures, where the liquid disappears more quickly, rapid grain growth would occur a smaller fraction of the sintering time and the time dependence of grain growth should deviate from that predicted by the model.

We propose, instead, that the rapid grain growth at higher metal loadings is controlled by a decrease in porosity; that is, grains can grow only when they are in contact with other grains. The grain size data in Fig. 7, then, are explained largely by the changes in porosity shown in Fig. 6.

The strong dependence of grain size and porosity on the Ti-TiC ratio appears to arise for two reasons. First, the green density decreases as the titanium content increases (Fig. 9) because at room temperature the titanium metal is relatively ductile (particularly in comparison to the brittle TiC). Second, rearrangement of TiC particles in the titanium liquid appears to be an important mechanism of densification. Densification due to solid-particle rearrangement during nonreactive liquid-phase sintering is a function of the volume of liquid [12]. Because the titanium metal in the present study rapidly reacts to form a carbide skeleton, densification by rearrangement of the carbide grains in the eutectic liquid is limited. The

particle rearrangement that occurs in the eutectic liquid before a carbide skeleton forms has the effect of changing the value of P as a function of composition. Because P was included in the function $A(C)$ in Equations 5 and 6, the empirical value of $A(C)$ also describes any changes of P due to initial solid-particle rearrangements. The fact that a solid carbide skeleton forms so rapidly in the titanium-titanium-carbide system permits the adaptation of Kuczynski's model for solid-state sintering to these data.

The activation energy for grain growth, and consequently for densification, 260 kJ M^{-1} , is similar to that measured for diffusion of carbon along grain boundaries and along TiC-Ti₂C interfaces [11, 13-16]. In the matrix Ti diffuses nearly five orders of magnitude more slowly than C and with an activation energy nearly twice that for carbon diffusion [17, 18]. Although no direct measure of grain boundary diffusion of Ti in TiC is available, tracer diffusion of niobium in polycrystalline TiC [19] suggests that metal and carbon atoms may diffuse at similar rates and with similar activation energies along grain boundaries.

Acknowledgements

Analyses of the starting powders and preparation of the sintered samples was carried out at the Sullivan Park Research Laboratories of Corning Glass Works. The transmission electron microscope was made available through the Central Facility for Electron Microscopy in the Materials Science Center at Cornell University. This work is supported by the Department of Energy under grant number DE-AC02-77ER04441 and by Corning Glass Works.

References

1. W. S. WILLIAMS, in "Progress in Solid State Chemistry", edited by H. Reiss and J. O. McCaldin (Pergamon, New York, 1971) p. 57.
2. L. E. TOTH, "Refractory Materials" Vol. 6, (Academic, New York, 1967) p. 1.
3. E. K. STORMS, "Refractory Materials" Vol. 2, (Academic, New York, 1967) p. 1.
4. G. C. KUCZYNSKI, in "Materials Science Research" Vol. 6, edited by G. C. Kuczynski (Plenum, New York, 1972) p. 217.
5. G. E. P. BOX and K. B. WILSON, *J. Roy. Statist. Soc.* **13** (1951) 455.
6. O. DAVIES, "Statistical Methods in Research and Production" (Oliver and Boyd, London, 1947) p. 47.
7. T. RYAN, B. JOINER and B. RYAN, "Minitab Reference Manual" (University of Pennsylvania Press, State College, 1981).
8. H. EXNER, *Int. Metall. Rev.* **159** (1978) 25.
9. K. FRYE, "Modern Mineralogy" (Prentice Hall, Englewood Cliffs, 1974) p. 159.
10. R. COBLE, in "Materials Science Research", Vol. 6, edited by G. C. Kuczynski, (Plenum, New York, 1972) 177.
11. C. J. QUINN and D. L. KOHLSTEDT, *J. Mater. Sci.* **19** (1984) 1242.
12. W. D. KINGERY, *J. Appl. Phys.* **30** (1959) 301.
13. L. M. ADELSBERG and L. H. CADOFF, *Trans. AIME* **239** (1967) 933.
14. C. VANSANT and W. PHELPS, *Trans. ASM* **59** (1966) 105.
15. D. L. KOHLSTEDT, W. S. WILLIAMS and J. B. WOODHOUSE, *J. Appl. Phys.* **41** (1970) 4476.
16. C. J. QUINN and D. L. KOHLSTEDT, *J. Amer. Ceram. Soc.* (1984).
17. S. SARIAN, *J. Appl. Phys.* **40** (1969) 3515.
18. *Idem, ibid.* **39** (1968) 3305.
19. K. TOKAR, H. OEL and A. ILLIGEN, *Ber. Deut. Karam. Ges.* **43** (1966) 163.

Received 27 June

and accepted 26 July 1983